The Inherent Representation of Tactile Manipulation Using Unified Force-Impedance Control

Kübra Karacan, Robin Jeanne Kirschner, Hamid Sadeghian, Fan Wu, and Sami Haddadin

***Abstract*— Different robotic manipulation tasks require different execution and planning strategies. Nevertheless, the versatility of tasks in assembly and disassembly demands flexible control strategies. Fundamental to achieving such adaptive control methods is understanding and generalizing the interactions between tools, the manipulated object, and the environment required to perform a manipulation. This paper addresses the problem of generating adaptive manipulation by introducing the force-velocity task phase plot that represents the inherent nature of tactile manipulation skills. This representation enables us to identify the primary phases of the interaction in the force-velocity domain. Using unified force-impedance control, we establish a tactile manipulation strategy to robustly conduct versatile manipulation tasks even in case of disturbances or imprecise task information. The proposed control scheme features a dynamic process for impedance shaping based on the external force applied to the robot and the skill motion error for collision response, as well as a force-shaping function that enables both a smooth transition from free motion to contact and force regulation. We implement and compare the control strategy to previously proposed strategies using peg-in-hole reference experiments that include force disturbance and positioning inaccuracies and show the respective task phase plots. As a result, we observe high controller robustness and conclude that using the task phase plot as the inherent representation of tactile manipulation via unified force-impedance control enables successful adaptive controller design and creates a quantifiable basis for robotic skill solution comparison.**

I. Introduction

Robotic manipulation plays a vital role in the digital transformation of traditional factories, enabling the automation of assembly and disassembly operations, e.g., for electronic waste recycling [1]. Robotic solutions to such processes require complex robot capabilities and robustness to varying conditions [2]–[4]. For example, the dismantling procedure for a battery from a heat cost allocator (see Fig. 1) includes

The authors are with the Chair of Robotics and Systems Intelligence, MIRMI-Munich Institute of Robotics and Machine Intelligence, Technical University of Munich, Germany, and also with the Centre for Tactile Internet with Human-in-the-Loop (CeTI). H. Sadeghian also has an affiliation with the University of Isfahan. We gratefully acknowledge the funding by the European Union's Horizon 2020 research and innovation program as part of the project ReconCycle under grant no. 871352, the Bavarian State Ministry for Economic Affairs, Regional Development and Energy (StMWi) for the Lighthouse Initiative KI.FABRIK, (Phase 1: Infrastructure as well as the research and development program under, grant no. DIK0249), LongLeif GaPa gGmbH (Geriatronics Project Y)and German Research Foundation (DFG, Deutsche Forschungsgemeinschaft) as part of Germany's Excellence Strategy – EXC 2050/1 – Project ID 390696704 – Cluster of Excellence "Centre for Tactile Internet with Human-in-the-Loop" (CeTI) of Technische Universität Dresden. The authors would like to thank the Bavarian State Ministry for Economic Affairs, Regional Development and Energy (StMWi) for financial support as part of the project SafeRoBAY (grant number: DIK0203/01). Please note that S. Haddadin has a potential conflict of interest as a shareholder of Franka Emika GmbH.

Corresponding Author: K. Karacan kuebra.karacan@tum.de

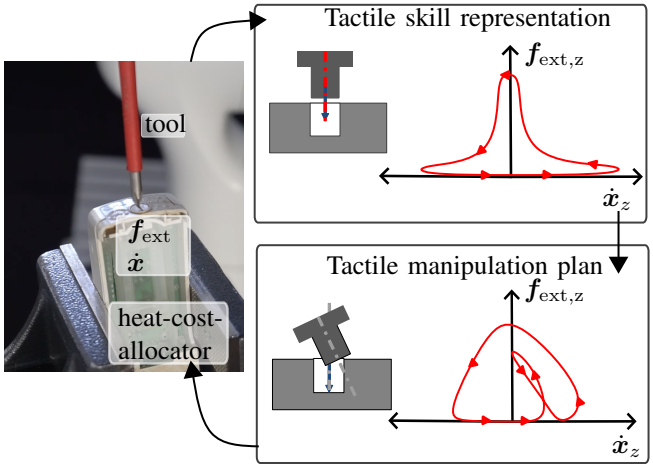

Fig. 1: **Pipeline from real-life application to tactile skill**. Understanding the underlying system of a tactile skill by simplified representations enables the derivation of manipulation plans that can cope with environmental uncertainties for successful task execution.

(i) placing the tool in contact with the gap (pre-contact and contact initiation); (ii) pushing the pin; (iii) levering the lid and PCB; and (iv) separating the battery [5]. To obtain a flexible automation solution to this versatile process, the location, and dimension of the region of interest, like the screw hole, can be obtained, e.g., by a camera. Even though such external sensing suffers from uncertainties and may provide imprecise positioning information, the robot should robustly align the tool with the contact to execute the desired tactile manipulation skills, such as pushing the pin, levering the lid, and cutting the battery. Thus, besides precise motion, a sense of touch has become crucial, which leads to the definition of tactile manipulation skills [6]–[8].

The introduction of torque-controlled tactile robots capable of perceiving touch enabled robotic skills that require force-motion commands and high compliance [9], [10]. To allow these skills, multiple strategies are available, e.g., admittance control [11], impedance control [12], force control [13], and even unified control [14]. Numerous studies consider force control as a solution to adaptive robotic skills, validating the suggested controllers using constant force values, thresholds, or limitations [15]–[19]. However, these strategies cannot cope with environmental uncertainties and may fail when faced with perception imprecision [20], [21]. Impedance control is a well-known technique that enforces dynamic behavior for interacting with the environment and the desired motion [12]. These dynamics can be achieved in the joint space, operational space, or even the null space of a robot manipulator [22]. Adaptive adjustment of impedance

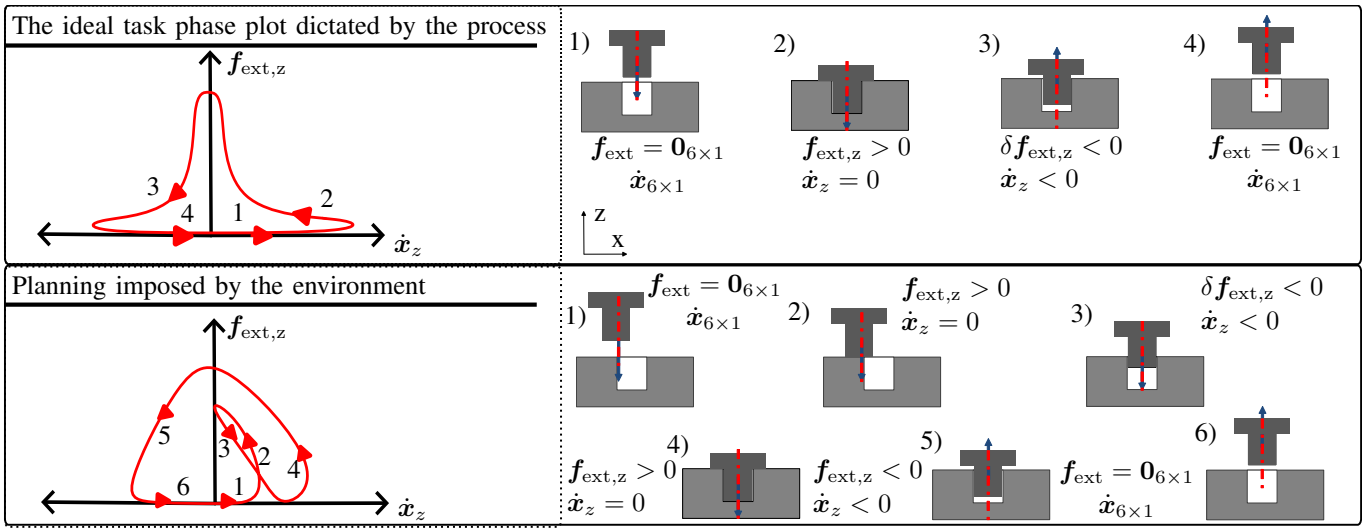

Fig. 2: **Tactile skill representation.** The task phase plot (f_{ext}, $\dot{x}$) is constrained by the desired state of the object, while the current environmental conditions form its shape. A manipulation plan should be devised to enable smooth transitions between the phases.

parameters is helpful in many applications [23], [24]. In applications with shared autonomy, variable impedance techniques are also utilized to coordinate the motions of humans and robots and update the desired skill motion policy [6]. Although the robotic community has been investigating adaptive manipulation with perception uncertainties so far, this is yet to be solved in principle and has not found its way into the industrial application domain [25]–[28]. Consequently, the field of electronic waste recycling is still primarily dominated by manual labor.

Successfully integrating adaptive robot manipulation skills represents a highly complex problem that consists of desired force and form closures between the robotic end-effector and the objects to be manipulated. Despite multiple attempts to solve adaptive manipulation, to the best of the authors' knowledge, a methodological approach to skill development starting with a formalism to represent the desired tactile manipulation strategy is yet missing. In this study, we derive a first representation of tactile skills based on unified force-impedance control, namely the *task phase plot*. It describes the entire cycle of a manipulation skill based on force and velocity information. Using unified force-impedance control, we use this formalism to develop a tactile manipulation strategy for robust contact initiation and flexible manipulation assuming inaccurate environmental information. The manipulation approach is designed dynamically, using impedance shaping to react to unforeseen contact and force-shaping to initiate and shape desired contact conditions. Using a peg-in-hole fitting experiment, we demonstrate the manipulation method and derive the task phase plots for comparison with state-of-the-art impedance and force controllers.

Additionally, we introduce the soft displacement metric that tests the robustness of the introduced manipulation strategy to position inaccuracies. We observe good positioning robustness and increased success of the introduced manipulation strategy compared to other solutions. Lastly, we present a possible extension of our controller for human-robot interaction

The paper is organized as follows. Section II introduces the inherent representation of tactile skills for robust contact initiation and flexible manipulation under environmental and positioning uncertainties, using unified force-impedance control. The experimental procedure and results are presented consecutively in Sec. III and Sec. IV. Finally, Sec. V concludes the paper.

II. Methodology

Physical interaction between two bodies requires robustly establishing and maintaining the desired contact by either force or form closure. Adapting to undesired contacts is one enabling factor in maintaining contact forces or achieving form fit. In this study, interaction skills that require motion and force policies and compliant behavior are referred to as *tactile manipulation skills*.

A. Tactile Skill Representation

Any tactile process such as peg-in-hole followed by releasing is defined with certain boundary conditions, i.e., motion and force. Ideally, the task phase plot, as shown in Fig. 2, demonstrates the entire cycle that the peg goes through, in which the force-velocity relation evolves:

1 - starting moving freely $f_{ext} = 0_{6\times1}$ toward the hole, while speeding up to $\dot{x}_{6\times1}$,
2 - smoothly establishing contact $\dot{x}_z = 0$ with the bottom surface, while an external force $f_{ext,z} > 0$ is exerted to it,
3 - breaking contact $\delta f_{ext,z} = 0$ while moving $\dot{x}_z$,
4 - back to the free condition $f_{ext,z}$ and $\dot{x}_z$.

However, the actual motion of the peg and the force exerted are formed based on force/wrench and twist constraints imposed by the environmental conditions, such as undesired contacts due to positioning imprecision. Here, the phases of tactile interaction repeat within the phase plot as contact is established multiple times before the desired goal state is achieved. Consequently, a tactile manipulation strategy is required to adapt the desired force and motion of the peg

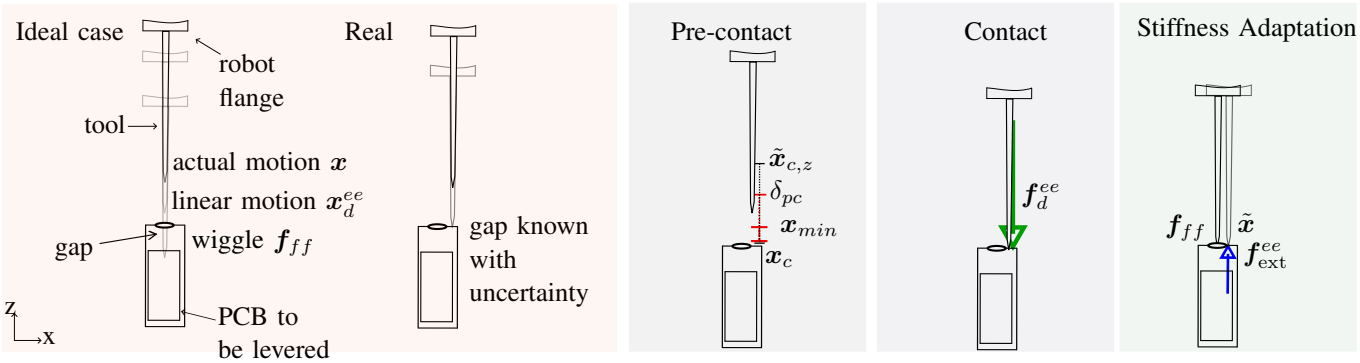

Fig. 3: **A simplified scheme of elements in the dismantling process of a heat cost allocator to recycle the battery.** The gap location $\boldsymbol{x}_c$ is assumed to be obtained externally. Impedance control is followed by desired motion $\boldsymbol{x}_d$. To insert the tool, a wiggle motion is applied via a feed-forward force $\boldsymbol{f}_{\text{ff}}$. When force control is activated, a desired force $\boldsymbol{f}_d$ establishes contact with the surface to make tool alignment possible. Stiffness adaptation enables the robot to have compliant behavior to adjust itself to the environment.

between the phases, leading to robust and successful task execution.

B. Tactile Manipulation Strategy

Using force-impedance control, we develop a tactile manipulation plan for robust contact initiation and flexible manipulation under positioning inaccuracies, as shown in the example of a peg-in-hole task for heat cost allocator disassembly in Fig. 3. First, we design a dynamic process for impedance shaping based on the external force exerted on the robot and the skill motion error to allow the robot to adjust its end-effector in response to incidental contact. Second, we create a force shaping function to enable (i) a smooth transition from free motion to contact (pre-contact shaping) and (ii) force regulation based on the desired tool alignment (contact shaping).

1) **Control design:** To control robot arm motion and force policies with n-DOF, the desired pose of the end-effector w.r.t. the robot base frame is $\boldsymbol{x}_d \in \mathbb{R}^6$. The robot's dynamics equation in Cartesian space in the base frame is

$$\boldsymbol{M}_C(\boldsymbol{q})\ddot{\boldsymbol{x}} + \boldsymbol{C}_C(\boldsymbol{q},\dot{\boldsymbol{q}})\dot{\boldsymbol{x}} + \boldsymbol{f}_g(\boldsymbol{q}) = \boldsymbol{f}_{\text{in}} + \boldsymbol{f}_{\text{ext}} \tag{1}$$

where $\boldsymbol{f}_{\text{ext}} \in \mathbb{R}^6$ is the external wrench w.r.t. the base frame. $\boldsymbol{M}_C(\boldsymbol{q})$ is the robot mass matrix, $\boldsymbol{C}_C(\boldsymbol{q},\dot{\boldsymbol{q}}) \in \mathbb{R}^{6\times6}$ is the Coriolis and centrifugal matrix, and $\boldsymbol{f}_g(\boldsymbol{q})$ is the gravity vector in Cartesian space. Furthermore, $\boldsymbol{f}_{\text{in}}$ is the wrench applied by the robot and relates to the joint control torque $\boldsymbol{\tau}_{\text{in}} \in \mathbb{R}^n$ by $\boldsymbol{\tau}_{\text{in}} = \boldsymbol{J}^T(\boldsymbol{q})\boldsymbol{f}_{\text{in}}$. Next, we design a control algorithm for the input torque $\boldsymbol{\tau}_{\text{in}}$ to perform the desired task. The proposed control law for adaptive tactile skills shown in Fig. 4 is extended from unified force-impedance control [6], [14] and comprises four main components:

I) tracking the desired motion $\boldsymbol{x}_d$ and adapting the robot stiffness level (ρ_{imp}) with impedance control,
II) applying feed-forward force $\boldsymbol{f}_{\text{ff}}$,
III) regulating the external force $\boldsymbol{f}_{\text{ext}}$ w.r.t. the desired force $\boldsymbol{f}_d$,
IV) gravity compensation for the robot.

The input torque $\boldsymbol{\tau}_{\text{in}} \in \mathbb{R}^n$ is:

$$\boldsymbol{\tau}_{\text{in}} = \boldsymbol{\tau}_{\text{imp}} + \boldsymbol{\tau}_{\text{ff}} + \boldsymbol{\tau}_{\text{frc}} + \boldsymbol{\tau}_g\,, \tag{2}$$

where $\boldsymbol{\tau}_{\text{imp}}$, $\boldsymbol{\tau}_{\text{ff}}$, $\boldsymbol{\tau}_{\text{frc}}$, and $\boldsymbol{\tau}_g \in \mathbb{R}^n$ are the input torques for (i) impedance control, (ii) feed-forward torque, (iii) force control, and (iv) gravity compensation.

2) **Variable impedance control:** The following control law is defined to establish the desired Cartesian impedance behavior on the tooltip.

$$\begin{aligned}\boldsymbol{\tau}_{\text{imp}} &= \boldsymbol{J}^T(\boldsymbol{q})(\boldsymbol{K}_C\tilde{\boldsymbol{x}} + \boldsymbol{D}_C\dot{\tilde{\boldsymbol{x}}} + \boldsymbol{M}_C(\boldsymbol{q})\ddot{\boldsymbol{x}}_d + \boldsymbol{C}_C(\boldsymbol{q},\dot{\boldsymbol{q}})\dot{\boldsymbol{x}}_d),\\ \tilde{\boldsymbol{x}} &= \boldsymbol{x}_d - \boldsymbol{x},\end{aligned} \tag{3}$$

where $\boldsymbol{x} \in \mathbb{R}^6$ is the actual pose of the end-effector in the base frame, and the pose error is $\tilde{\boldsymbol{x}}$. Moreover, $\boldsymbol{K}_C$ and $\boldsymbol{D}_C \in \mathbb{R}^{6\times6}$ are diagonal stiffness and damping matrices, respectively. The desired Cartesian inertia is assumed to be the robot inertia in Cartesian space. The difference between the desired and actual contact leads to a deviation from the desired pose $\boldsymbol{x}_d$, which alters $\tilde{\boldsymbol{x}}$, or the exerted force $\boldsymbol{f}_{\text{ext}}$. Therefore, we use a metric h to adapt the stiffness matrix $\boldsymbol{K}_{\text{C}}$ in impedance control according to the external force and the pose error:

$$S = \|\boldsymbol{f}_{\text{ext}}^T\tilde{\boldsymbol{x}}\|\,, \tag{4}$$

$$h = 1 - \frac{S}{S_{\text{t}}}\,. \tag{5}$$

Here, having the threshold S_{t} is crucial to compensate for minor effects of the environment, i.e., surface friction and measurement error [1]. The h is then coupled to $\boldsymbol{K}_{\text{C}}$ via ρ_{imp}:

$$\boldsymbol{K}_C = \rho_{\text{imp}}(t)\boldsymbol{K}_{\max}\,, \tag{6}$$

where the adaptation parameter ρ_{imp} is obtained by

$$\dot{\rho}_{\text{imp}} = \begin{cases}\min\{\rho,0\}\,, & \rho_{\text{imp}} = 1\\ \rho\,, & 0 < \rho_{\text{imp}} < 1,\ \rho_{\text{imp}}(0) = 0,\\ \max\{\rho,0\}\,, & \rho_{\text{imp}} = 0\end{cases} \tag{7}$$

and ρ is given by

$$\rho = h\rho_{\text{imp}} + \rho_{min}. \tag{8}$$

Note that, to have an initial increment for the case $\rho_{\text{imp}} = 0$, a small positive constant ρ_{min} has been introduced into the shaping function dynamics.

[1]Please note that using pose instead of velocity or acceleration leads to having a comparably less noisy signal

3) **Force control:** The force control is defined to maintain the desired contact force $\boldsymbol{f}_{\mathrm{d}}^{\mathrm{ee}} \in \mathbb{R}^6$ applied by the robot w.r.t. the external force $\boldsymbol{f}_{\mathrm{ext}}^{\mathrm{ee}} \in \mathbb{R}^6$ as follows

$$\boldsymbol{\tau}_{\mathrm{frc}} = \rho_{\mathrm{frc}} \boldsymbol{J}(\boldsymbol{q})^T \boldsymbol{f}_{\mathrm{frc}}, \tag{9}$$

$$\boldsymbol{f}_{\mathrm{frc}} = \begin{bmatrix} [\boldsymbol{R}_{\mathrm{ee}}^{\mathrm{O}}]_{3\times3} & \boldsymbol{0}_{3\times3} \\ \boldsymbol{0}_{3\times3} & [\boldsymbol{R}_{\mathrm{ee}}^{\mathrm{O}}]_{3\times3} \end{bmatrix} (\boldsymbol{f}_d^{\mathrm{ee}} + \boldsymbol{K}_p\, \tilde{\boldsymbol{f}}_{\mathrm{ext}}^{\mathrm{ee}} + \boldsymbol{K}_i \int \tilde{\boldsymbol{f}}_{\mathrm{ext}}^{\mathrm{ee}}\, dt + \boldsymbol{K}_d\, \dot{\tilde{\boldsymbol{f}}}_{\mathrm{ext}}^{\mathrm{ee}}), \tag{10}$$

$$\tilde{\boldsymbol{f}}_{\mathrm{ext}}^{\mathrm{ee}} = \boldsymbol{f}_d^{\mathrm{ee}} + \boldsymbol{f}_{\mathrm{ext}}^{\mathrm{ee}}, \tag{11}$$

where $\boldsymbol{f}_{\mathrm{frc}} \in \mathbb{R}^6$ is a feedback force controller in the base frame rotated by $\boldsymbol{R}_{\mathrm{ee}}^{\mathrm{O}}$. The PID controller gains are the diagonal matrices of $\boldsymbol{K}_p$, $\boldsymbol{K}_i$, $\boldsymbol{K}_d \in \mathbb{R}^{6\times6}$. Moreover, the force shaping function ρ_{frc} decides to activate or deactivate the force controller based on the defined conditions

$$\rho_{\mathrm{frc}} = \rho_{\mathrm{imp}} \rho_{\mathrm{pc}} \rho_{\mathrm{c}}\,. \tag{12}$$

To avoid phase switching, we define the force shaping function ρ_{frc} by combining ρ_{pc} and ρ_{c}. When the tool is close to the desired contact surface by $\delta_{\mathrm{pc}} > 0$, force control is activated smoothly, and its weight is equal to one at $\boldsymbol{x}_{\min}$. During the contact, the robot tolerates the tool alignment error up to a certain threshold of $\delta_{\mathrm{c}} > 0$. For instance, force control is deactivated if the robot loses contact with the surface due to a large tool alignment error. Thus, the robot becomes only impedance-controlled and tracks the desired motion. Pre-contact shaping ρ_{pc} is designed based on the distance between the tool and the desired contact surface in the z-direction in the task frame $\tilde{\boldsymbol{x}}_{\mathrm{c}} = \boldsymbol{x}_{\mathrm{c}} - \boldsymbol{x}$:

$$\rho_{\mathrm{pc}} = \begin{cases} 1\,, & x_{\min} \le \tilde{\boldsymbol{x}}_{\mathrm{c,z}} \\ \frac{1}{2}(1 + \cos((\frac{x_{\min} - \tilde{\boldsymbol{x}}_{\mathrm{c,z}}}{\delta_{\mathrm{pc}}})\pi))\,, & x_{\min} > \tilde{\boldsymbol{x}}_{\mathrm{c,z}} \ge x_{\min} - \delta_{\mathrm{pc}} \\ 0\,, & \text{otherwise.} \end{cases} \tag{13}$$

Contact shaping ρ_{c} as a function of tool alignment error $\boldsymbol{f}_{\mathrm{d}}^T \tilde{\boldsymbol{x}}$ by bounding it with the limits of $S_{\min}$ and $\delta_{\mathrm{c}} > 0$:

$$\rho_{\mathrm{c}} = \begin{cases} 1\,, & \boldsymbol{f}_{\mathrm{d}}^T \tilde{\boldsymbol{x}}_{\mathrm{c}} \le S_{\min} \\ \frac{1}{2}(1 + \cos((\frac{\boldsymbol{f}_{\mathrm{d}}^T \tilde{\boldsymbol{x}}_{\mathrm{c}} - S_{\min}}{\delta_{\mathrm{c}}})\pi))\,, & S_{\min} < \boldsymbol{f}_{\mathrm{d}}^T \tilde{\boldsymbol{x}}_{\mathrm{c}} \le S_{\min} + \delta_{\mathrm{c}} \\ 0\,, & \text{otherwise.} \end{cases} \tag{14}$$

When the robot is fully compliant $\rho_{imp} = 0$, it becomes adjustable to the environment. After reaching its maximum stiffness, the robot is adapted to the current environmental conditions and restarts the desired motion from its current configuration.

Finally, the closed-loop equation for the overall system becomes the following

$$\boldsymbol{M}_C(\boldsymbol{q})\ddot{\tilde{\boldsymbol{x}}} + \boldsymbol{C}_C(\boldsymbol{q}, \dot{\boldsymbol{q}})\dot{\tilde{\boldsymbol{x}}} + \boldsymbol{D}_C\dot{\tilde{\boldsymbol{x}}} + \boldsymbol{K}_C\tilde{\boldsymbol{x}} + \boldsymbol{f}_{\mathrm{frc}} + \boldsymbol{f}_{\mathrm{ff}} + \boldsymbol{f}_{\mathrm{ext}} = 0\,. \tag{15}$$

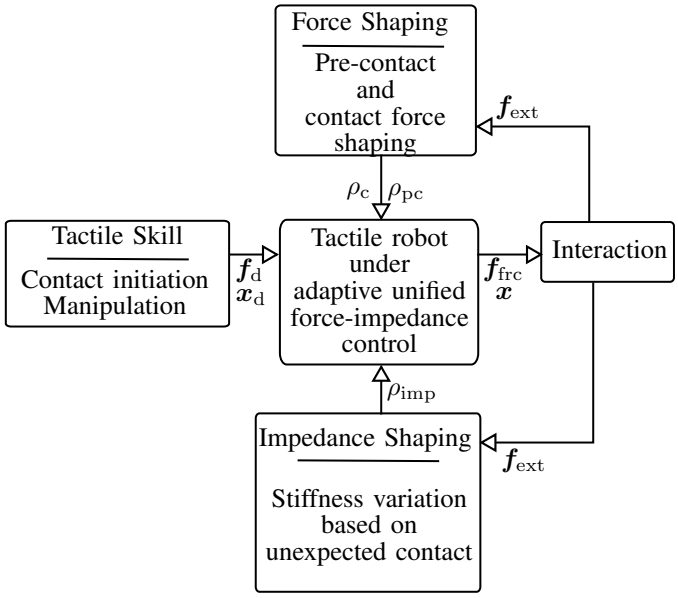

Fig. 4: **Tactile manipulation strategy.** The controller shaping functions ensure robust and safe interaction with the environment.

In addition, to ensure controller stability, which might be compromised due to variable impedance [29], the Lyapunov candidate function is

$$V = \frac{1}{2}\dot{\tilde{\boldsymbol{x}}}^T \boldsymbol{M}_C \dot{\tilde{\boldsymbol{x}}} + \frac{1}{2}\tilde{\boldsymbol{x}}^T \boldsymbol{K}_C \tilde{\boldsymbol{x}}\,. \tag{16}$$

Differentiating V and rearranging the corresponding terms for $\boldsymbol{f}_{\mathrm{ext}} = 0$ and the constant $\boldsymbol{M}_C$ result in

$$\dot{V} = -\dot{\tilde{\boldsymbol{x}}}^T \boldsymbol{D}_C \dot{\tilde{\boldsymbol{x}}} + \frac{1}{2}\tilde{\boldsymbol{x}}^T \dot{\boldsymbol{K}}_C \tilde{\boldsymbol{x}}\,. \tag{17}$$

Due to the term $\dot{\boldsymbol{K}}_C$, the eigenvalues of the stiffness matrix $\boldsymbol{K}_C$ should be constant or decreasing for $\tilde{\boldsymbol{x}} \neq 0$. It can be deduced from Eq. 6 that the rate of change of the stiffness matrix $\dot{\boldsymbol{K}}_C$ is directly proportional to the rate of change of the adaption parameter $\dot{\rho}_{\mathrm{imp}}$:

$$\dot{\boldsymbol{K}}_C = \dot{\rho}_{\mathrm{imp}} \boldsymbol{K}_{\max}\,. \tag{18}$$

Furthermore, once the motion error $\tilde{\boldsymbol{x}}$ exceeds defined thresholds in Eq. 4, 5, and 8, by the definition of $\dot{\rho}_{\mathrm{imp}} = \min\{\rho, 0\}$ in Eq. 7, $\boldsymbol{K}_C$ decreases due to $\dot{\rho}_{\mathrm{imp}} < 0$. Stiffness $\boldsymbol{K}_C$ increases again; only the motion error and external force are within the thresholds. Briefly, while the motion error $\tilde{\boldsymbol{x}}$ exists, the stiffness $\boldsymbol{K}_C$ decreases:

$$\boldsymbol{K}_{\mathrm{C}} = \begin{cases} \text{constant stiffness } \mathrm{K}_{\max}, & \rho_{\mathrm{imp}} = 1 \ \wedge \tilde{\boldsymbol{x}} = 0 \\ \text{decreases}, & \tilde{\boldsymbol{x}} \neq 0 \\ \text{increases to } \mathrm{K}_{\max}, & \rho_{\mathrm{imp}} \neq 1 \ \wedge \tilde{\boldsymbol{x}} = 0 \end{cases} \tag{19}$$

Please note that one might also install virtual energy tanks to ensure the passivity of the whole system as a sufficient condition to achieve stability [30].

TABLE I: Control parameters used in the experiments.

Parameter	Unit	Value
$\dot{\boldsymbol{x}}_z$	m/s	0.002
$\boldsymbol{K}_{\mathrm{x,imp}}$ and $\boldsymbol{K}_{\mathrm{x,afic}}$	N/m	diag[1000, 1000, 1000, 150, 150, 150]
$\boldsymbol{\xi}$	Ns/m	diag[0.7, 0.7, 0.7, 1, 1, 1]
$\boldsymbol{f}_{\mathrm{d}}^{\mathrm{ee}}$	N	[0, 0, 10, 0, 0, 0]
$\boldsymbol{K}_p, \boldsymbol{K}_i, \boldsymbol{K}_d$	$-$	$2.0\boldsymbol{I}_{6\times6}, 1.0\boldsymbol{I}_{6\times6}, 0\boldsymbol{I}_{6\times6}$
$\boldsymbol{K}_{\mathrm{x,fic}}$	N/m	diag[1000, 1000, 100, 150, 150, 150]
S_{t}	Nm	1.0
δ_{pc}	m	0.002
δ_{c}	Nm	0.5
$x_{\min}$	m	-0.001
$S_{\min}$	Nm	0.002

III. Experimental Validation

In particular, the protocol for recycling the battery from a heat cost allocator is: (i) placing the tool in contact with the gap (pre-contact and contact initiation); (ii) pushing the pin; (iii) levering the lid and PCB, and (iv) separating the battery. In a simplified form, the requirements of the dismantling protocol are (i) contact initiation, going to the gap with a specific orientation; (ii) establishing contact, tool alignment with the desired contact (gap); and (iii) manipulation: force and motion profile. Finally, the task performance is evaluated regarding position accuracy, motion profile error, force tolerance, force profile error, and compliance. We formulate contact initiation and establish contact under perception uncertainties as a peg-in-hole problem to obtain a reproducible reference setup to measure the controller performances. A Franka Emika robot is used for the experiments, and the robot's internal sensing records the position, velocity, and external end-effector force.

A. Contact Initiation: Peg-in-hole

A peg manufactured with fitting tolerance ($< 0.1\,\mathrm{mm}$) can be inserted via wiggle motion. In experiments, wiggle motion is realized by adding a feed-forward force term to the controller as a function of amplitude $a = -3\,\mathrm{N}$, frequency $\omega = 3\,\mathrm{Hz}$, and time t,

$$\boldsymbol{f}_{\mathrm{ff}} = [0, a\cos(2\pi\omega t), 0, 0, 0, 0]\,. \tag{20}$$

The length and diameter of the peg are $20\,\mathrm{mm}$ and $3\,\mathrm{mm}$, respectively.

Experiment 1: In the first set of experiments, four different control methods are compared: (i) impedance, (ii) force, (iii) force-impedance, and (iv) adaptive force-impedance control. The robot starts with non-contact $2\,\mathrm{mm}$ above the hole. Afterward, it freely moves and establishes contact. Finally, the robot is expected to insert the peg until it is in contact with the bottom of the hole. The control parameters used in the experiments are listed in Tab. I.

Experiment 2: The application of force-impedance control promises to enable coping with displacement imprecision, especially for interaction tasks. We introduce the *soft displacement* metric to quantify this capability. This metric analyses the displacement from the ideal insertion line for a peg-in-hole application starting from which the peg-in-hole operation is still successful based on robot compliance. The time to complete the task and the peak forces can be used to evaluate the controller's quality. In the experiment, the initial robot position $\boldsymbol{x}_0$ is displaced towards the location of the hole, $\boldsymbol{x}_{\mathrm{c}}$, by $\delta_{\mathrm{pc}} = 2\,\mathrm{mm}$ in the z-direction:

$$\boldsymbol{x}_{\mathrm{c,z}} = \boldsymbol{x}_{0,\mathrm{z}} - \delta_{\mathrm{pc}}\,. \tag{21}$$

Once the robot is compliant, the initial pose is updated with the current pose. Thus, the robot reactivates the force controller within the defined thresholds. The experiments are repeated three times, using the displacements 3, 9, and $15\,\mathrm{mm}$ in the y-direction successively.

Experiment 3: We present a possible use case for our method in human-robot interaction to enable collaborative working. The impedance shaping function decreases the robot's stiffness when a human applies force. Using this compliant behavior, the human expert puts the robot into another contact, and then the robot is expected to insert the peg.

IV. Results and Discussion

The following section presents our experimental results in order of the three conducted experiments. All results are plotted based on the distance between the initial and current end-effector position w.r.t the base frame. As the peg length is of $20\,\mathrm{mm}$, it is also the maximum distance the robot may travel in the z-direction. Therefore, if $20\,\mathrm{mm}$ distance along the z-direction and an approximate velocity of $0\,\mathrm{mm/s}$ are reached, we rate the task completion as successful. Additionally, the task phase plot is developed with the external force and velocity in the z-direction, which also translates to the power evolution during the task. It is presented in the robot task space.

The results of position and force over time and the task phase plots for **Experiment 1** are shown in Fig. 5.

For controller the impedance controller, Fig. 5a), at first, the wiggle motion is dominant in the position plot. Then, the insertion starts, and the corresponding external forces increase. The robot successfully inserts the peg after $13\,\mathrm{s}$. However, there is no significant contact force until after $10\,\mathrm{s}$, the robot senses the external force due to tolerance adjustment during insertion. After hitting the bottom of the hole, the robot measures a force value of around $10\,\mathrm{N}$. Moreover, as there is no specified goal, the robot tries to move further at the bottom and gives a Cartesian reflex error.

Using the force controller shows that the robot controls the force well below the desired maximum of $10\,\mathrm{N}$, Fig. 5b). However, as can be seen in the task phase and position plot, the robot fails to slow down and gives an error after $0.2\,\mathrm{s}$ due to embedded safety around $150\,\mathrm{mm/s}$.

Next, in Fig. 5c) unified force-impedance control is applied, which commands low stiffness in the insertion direction to utilize compliant behavior as well as the tactility of the robot. Similarly to the force controller results, the force-impedance controlled force stays mainly below the

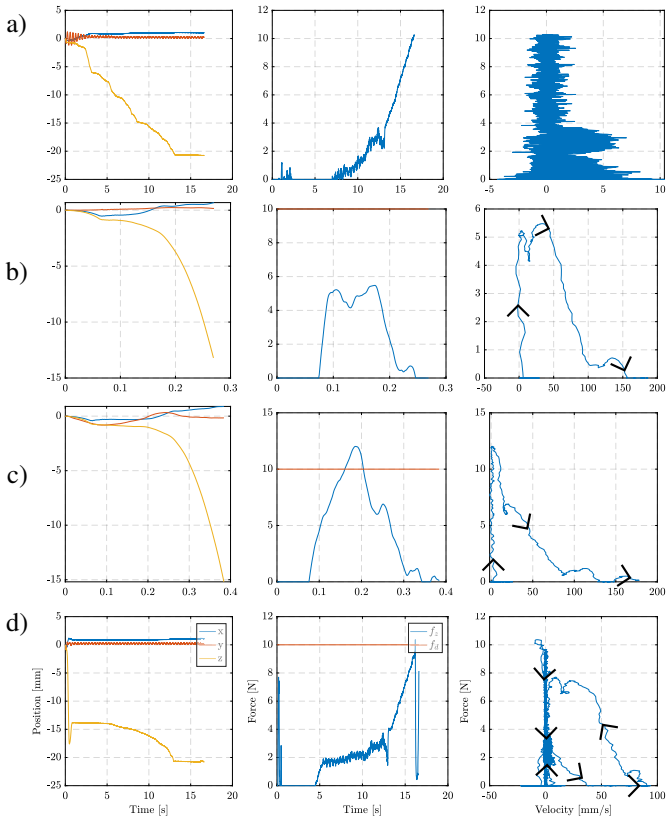

Fig. 5: **Results of Experiment 1: Comparative results for different controllers.** Position (current distance to the initial position in the x, y, and z direction in the base frame) vs. time, force in the z-direction in the task frame vs. time, and force in the z-direction in the task frame vs. velocity in the task frame (task phase plot) Arrows proceed in time. a) Impedance control b) Force control with $10\,\mathrm{N}$ in the z-direction c) Force impedance control with $10\,\mathrm{N}$ in the z-direction d) Adaptive force impedance control with $10\,\mathrm{N}$ in the z-direction

desired threshold, besides a short overshoot with $0.05\,\mathrm{s}$ duration. Nevertheless, just like the force controller, the force-impedance control cannot close the loop in the task phase plot without a specified end condition.

Finally, unified force-impedance control with adaptive stiffness is tested, shown in Fig. Fig. 5d). If there is no contact, the controller acts as pure impedance control. When the robot is close to the hole by δ_{pc}, force control is activated, and its weight reaches 1 after $\boldsymbol{x}_{\mathrm{min}}$. When the peg enters the hole without obstruction, as there is no contact to maintain due to the tool alignment error, the force control's weight decreases. Thus, the robot becomes only impedance-controlled and tracks the desired linear motion in the z-direction. Whenever the robot reaches the bottom, it stops due to the low stiffness, as seen in the task phase plot.

Using adaptive force-impedance control, in **Experiment 2**, we observe how compliant behavior allows to correct previous robot tool displacement of varying distances to achieve the peg-in-hole even if the robot is imperfectly positioned, as shown in Fig. 6.

Overall, in all cases, the peg-in-hole task is successfully conducted, regardless of the initial displacement of 0, 3, 9, or $15\,\mathrm{mm}$ as shown in Fig. 6 a), b), c), and d), respectively. In the position plot, the robot's motion along the y-direction shows the distance from the hole where the robot starts to move. The robot begins the wiggle motion, and the stiffness becomes low due to external force and motion error. Using the momentum caused by the feed-forward force, the robot moves towards the hole compliantly. Notably, the direction of the feed-forward force influences the soft displacement experiments, and it should be towards the hole. This procedure repeats until the robot reaches the desired contact at the bottom of the hole.

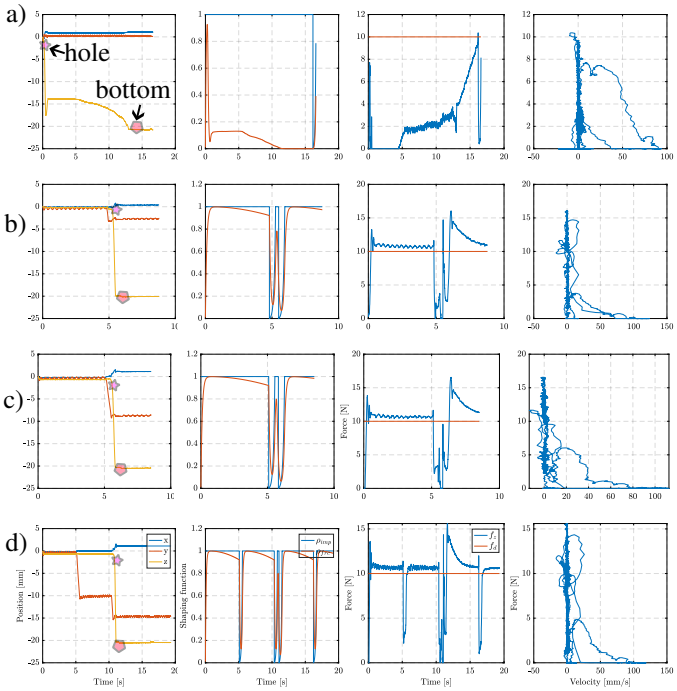

Fig. 6: **Results of Experiment 2: Soft displacement.** Using adaptive force-impedance control, starting at various distances in the y direction in the base frame to the center of the hole. Position (current distance to the initial position in the x, y, and z-direction in the base frame) vs. time, force-impedance shaping function vs. time, force in the z-direction in the task frame vs. time, and force in the z-direction in the task frame vs. velocity in the task frame (task phase plot) a) $0\,\mathrm{mm}$ b) $3\,\mathrm{mm}$ c) $9\,\mathrm{mm}$ d) $15\,\mathrm{mm}$

In **Experiment 3**, the robot encounters an additional contact with the human operator while inserting the peg, shown in Fig. 6. At this contact, the robot becomes compliant again owing to stiffness adaptation. After this contact is released, the robot adjusts to the new environment and updates the initial position with the current one. The force control is again activated to maintain contact up to a certain threshold δ_{c}, as shown in the force plots in Fig. 6b), c), and d). This helps the robot restart applying force as we choose the desired contact $2\,\mathrm{mm}$ away from the initial position. In other words, the robot can perceive touch as a human does with a fingertip.

Incidental contact with the human expert leads to a decrease in the robot's stiffness. Thus, the human moves the robot to another region of interest as if in guiding mode. The human expert puts the robot into another contact to insert the

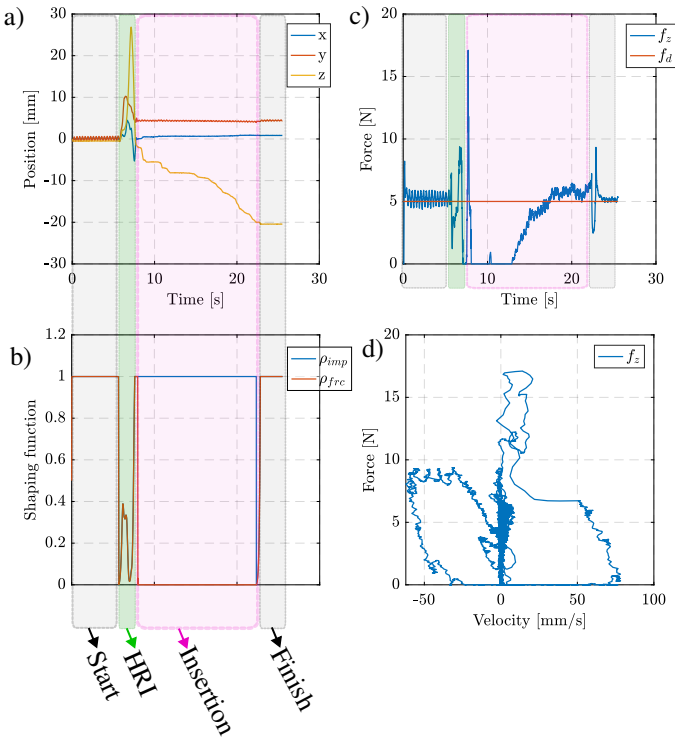

Fig. 7: **Results of Experiment 3: Results for human-robot interaction using adaptive unified force-impedance control** a) Distance between the end-effector's current and initial position in x, y, and z-direction b) Force-Impedance shaping functions c) Force vs. time d) Task phase plot

peg, as shown in Fig.7. According to ISO 15066, the robot's velocity can be considered within the safe limits for hand-guided human-robot collaboration $(250\,\mathrm{mm/s})$ [31].

The limitation of the presented control scheme is to design the control parameters wisely beforehand. For instance, δ_{pc} should not be smaller than the vertical distance to the surface.

V. Conclusion

Digital transformation of traditional factories requires robots to perform tactile skills under varying conditions. However, a tactile manipulation strategy is yet to be developed to handle unexpected situations and inaccurate environment models. Therefore, we propose designing such a manipulation strategy by analysis of the underlying system. For that, we apply the inherent representation of manipulation tasks, namely the force-velocity task phase plot, to identify relevant phases and enable the design of controllers that can smoothly adapt between these phases. Based on this representation, we design a unified force-impedance control method for reliable contact initiation and flexible manipulation under positioning and environmental uncertainties. First, based on the external force applied to the robot and the skill motion error, we design a dynamic process for impedance shaping to enable the robot to adjust its end-effector in response to unforeseen contact. Second, we establish a force shaping function that includes (i) a smooth transition from free motion to contact (pre-contact shaping) and (ii) force regulation based on the desired tool alignment (contact shaping). Third, to compare our results with a reference setup, we observe our control scheme's capability to succeed in the desired task under positioning inaccuracy using the example of a peg-in-hole skill.

Furthermore, we compare four controllers to evaluate the success rate based on their respective task phase plots. As a result of the controller comparison, the importance of commanding force and motion policies with compliant behavior becomes apparent. Finally, we show how our force-impedance shaping in unified force-impedance control increases robustness for contact initiation and flexibility during manipulation. We also demonstrate a potential extension of our method to human-robot interaction.

The presented work shows the potential of the force-velocity task phase plot as a foundation for robotic skill design and comparison based on peg-in-hole insertion and removal. Future work will investigate in depth the applicability of this manipulation representation for creating versatile tasks.

References

[1] A. Lambert and S. Gupta, "Disassembly modeling for assembly, maintenance, reuse and recycling," 12 2004.

[2] E. Garcia, M. A. Jimenez, P. G. De Santos, and M. Armada, "The evolution of robotics research," *IEEE Robotics & Automation Magazine*, vol. 14, no. 1, pp. 90–103, 2007.

[3] A. Billard and D. Kragic, "Trends and challenges in robot manipulation," *Science*, vol. 364, no. 6446, p. eaat8414, 2019. [Online]. Available: https://www.science.org/doi/abs/10.1126/science.aat8414

[4] S. Haddadin, L. Johannsmeier, and F. Díaz Ledezma, "Tactile robots as a central embodiment of the tactile internet," in *Proceedings of the IEEE*, vol. 107, no. 2, Feb. 2019, pp. 471–487.

[5] M. Simonič;, R. Pahič;, T. Gašpar, S. Abdolshah, S. Haddadin, M. G. Catalano, F. Wörgötter, and A. Ude, "Modular ros-based software architecture for reconfigurable, industry 4.0 compatible robotic workcells," in *2021 20th International Conference on Advanced Robotics (ICAR)*, Dec 2021, pp. 44–51.

[6] K. Karacan, H. Sadeghian, R. Kirschner, and S. Haddadin, "Passivity-based skill motion learning in stiffness-adaptive unified force-impedance control," in *2022 IEEE/RSJ International Conference on Intelligent Robots and Systems (IROS)*, Oct 2022, pp. 9604–9611.

[7] J. Lloyd and N. F. Lepora, "Goal-driven robotic pushing using tactile and proprioceptive feedback," *IEEE Transactions on Robotics*, vol. 38, no. 2, pp. 1201–1212, 2022.

[8] K. Karacan, D. Grover, H. Sadeghian, F. Wu, and S. Haddadin, "Tactile exploration using unified force-impedance control," Jul 2023, p. under publication, 22nd IFAC World Congress.

[9] S. Haddadin, S. Parusel, L. Johannsmeier, S. Golz, S. Gabl, F. Walch, M. Sabaghian, C. Jähne, L. Hausperger, and S. Haddadin, "The franka emika robot: A reference platform for robotics research and education," *IEEE Robotics & Automation Magazine*, vol. 29, no. 2, pp. 46–64, 2022.

[10] R. J. Kirschner, A. Kurdas, K. Karacan, P. Junge, S. Birjandi, N. Mansfeld, S. Abdolshah, and S. Haddadin, "Towards a reference framework for tactile robot performance and safety benchmarking," in *2021 IEEE/RSJ International Conference on Intelligent Robots and Systems (IROS)*. IEEE, 2021, pp. 4290–4297.

[11] E. Shahriari, A. Kramberger, A. Gams, A. Ude, and S. Haddadin, "Adapting to contacts: Energy tanks and task energy for passivity-based dynamic movement primitives," in *2017 IEEE-RAS 17th International Conference on Humanoid Robotics (Humanoids)*. IEEE, 2017, pp. 136–142.

[12] N. Hogan, "Impedance control: An approach to manipulation," in *1984 American Control Conference*, 1984, pp. 304–313.

[13] O. Khatib, "A unified approach for motion and force control of robot manipulators: The operational space formulation," *IEEE J. Robotics Autom.*, vol. 3, pp. 43–53, 1987.

[14] C. Schindlbeck and S. Haddadin, "Unified Passivity-Based Cartesian Force / Impedance Control for Rigid and Flexible Joint Robots via Task-Energy Tanks," *2015 IEEE International Conference on Robotics and Automation (ICRA)*, pp. 440–447, 2015.

[15] A. Cherubini, R. Passama, A. Crosnier, A. Lasnier, and P. Fraisse, "Collaborative manufacturing with physical human–robot interaction," *Robotics and Computer-Integrated Manufacturing*, vol. 40, pp. 1–13, 2016. [Online]. Available: https://www.sciencedirect.com/science/article/pii/S0736584515301769

[16] F. Ficuciello, L. Villani, and B. Siciliano, "Variable impedance control of redundant manipulators for intuitive human–robot physical interaction," *IEEE Transactions on Robotics*, vol. 31, no. 4, pp. 850–863, Aug 2015.

[17] W. He, Y. Chen, and Z. Yin, "Adaptive neural network control of an uncertain robot with full-state constraints," *IEEE Transactions on Cybernetics*, vol. 46, no. 3, pp. 620–629, March 2016.

[18] F. Kulakov, G. V. Alferov, P. Efimova, S. Chernakova, and D. Shymanchuk, "Modeling and control of robot manipulators with the constraints at the moving objects," in *2015 International Conference "Stability and Control Processes" in Memory of V.I. Zubov (SCP)*, Oct 2015, pp. 102–105.

[19] C. Ott, A. Dietrich, and A. Albu-Schäffer, "Prioritized multi-task compliance control of redundant manipulators," *Automatica*, vol. 53, pp. 416–423, 2015. [Online]. Available: https://www.sciencedirect.com/science/article/pii/S0005109815000163

[20] P. Pastor, M. Kalakrishnan, L. Righetti, and S. Schaal, "Towards associative skill memories," in *2012 12th IEEE-RAS International Conference on Humanoid Robots (Humanoids 2012)*, Nov 2012, pp. 309–315.

[21] A. Kramberger, A. Gams, B. Nemec, C. Schou, D. Chrysostomou, O. Madsen, and A. Ude, "Transfer of contact skills to new environmental conditions," in *2016 IEEE-RAS 16th International Conference on Humanoid Robots (Humanoids)*, 2016, pp. 668–675.

[22] H. Sadeghian, L. Villani, M. Keshmiri, and B. Siciliano, "Task-space control of robot manipulators with null-space compliance," *IEEE Transactions on Robotics*, vol. 30, no. 2, pp. 493–506, 2013.

[23] C. Yang, G. Ganesh, S. Haddadin, S. Parusel, A. Albu-Schaeffer, and E. Burdet, "Human-like adaptation of force and impedance in stable and unstable interactions," *IEEE transactions on robotics*, vol. 27, no. 5, pp. 918–930, 2011.

[24] F. J. Abu-Dakka and M. Saveriano, "Variable impedance control and learning—a review," *Frontiers in Robotics and AI*, vol. 7, 2020. [Online]. Available: https://www.frontiersin.org/articles/10.3389/frobt.2020.590681

[25] P. Pastor, M. Kalakrishnan, S. Chitta, E. Theodorou, and S. Schaal, "Skill learning and task outcome prediction for manipulation," in *2011 IEEE International Conference on Robotics and Automation*, May 2011, pp. 3828–3834.

[26] F. Ruggiero, V. Lippiello, and B. Siciliano, "Nonprehensile dynamic manipulation: A survey," *IEEE Robotics and Automation Letters*, vol. 3, no. 3, pp. 1711–1718, 2018.

[27] M. Qin, J. Brawer, and B. Scassellati, "Robot tool use: A survey," *Frontiers in Robotics and AI*, vol. 9, 2023. [Online]. Available: https://www.frontiersin.org/articles/10.3389/frobt.2022.1009488

[28] M. Suomalainen, Y. Karayiannidis, and V. Kyrki, "A survey of robot manipulation in contact," *Robotics and Autonomous Systems*, vol. 156, p. 104224, 2022. [Online]. Available: https://www.sciencedirect.com/science/article/pii/S0921889022001312

[29] K. Kronander and A. Billard, "Stability considerations for variable impedance control," *IEEE Transactions on Robotics*, vol. 32, no. 5, pp. 1298–1305, 2016.

[30] E. Shahriari, S. A. B. Birjandi, and S. Haddadin, "Passivity-based adaptive force-impedance control for modular multi-manual object manipulation," *IEEE Robotics Autom. Lett.*, vol. 7, no. 2, pp. 2194–2201, 2022. [Online]. Available: https://doi.org/10.1109/LRA.2022.3142903

[31] DIN ISO/TS 15066:2016-02, Robots and robotic devices — Collaborative robots (ISO/TS 15066:2016).